Nitride layer screening as carrier-selective contacts for silicon heterojunction solar cells

Angela N. Fioretti, Mathieu Boccard, Adele C. Tamboli, Andriy Zakutayev, and Christophe Ballif

Citation: AIP Conference Proceedings **1999**, 040007 (2018); doi: 10.1063/1.5049270
View online: https://doi.org/10.1063/1.5049270
View Table of Contents: http://aip.scitation.org/toc/apc/1999/1
Published by the American Institute of Physics

Nitride Layer Screening as Carrier-Selective Contacts for Silicon Heterojunction Solar Cells

Angela N. Fioretti,[1,2] Mathieu Boccard,[1, a)] Adele C. Tamboli,[2] Andriy Zakutayev,[2] Christophe Ballif[1]

[1] *Photovoltaics and Thin Film Electronics Laboratory, Institute of Microengineering, École Polytechnique Fédérale de Lausanne (EPFL), Rue de la Maladière 71b, CH-2000 Neuchâtel, Switzerland.*
[2]*National Renewable Energy Laboratory, 15013 Denver West Parkway, Golden, Colorado, USA 80401*

[a)]Corresponding author: mathieu.boccard@epfl.ch

Abstract. A three-architecture method for screening new materials' viability as carrier-selective contacts for silicon solar cells is presented. Test-structure solar cells were fabricated with a standard silicon heterojunction contact for the front side, and one of three treatments on the back: bare silicon, intrinsic amorphous silicon (i-aSi:H), or n-type amorphous silicon on an i-aSi:H passivation layer. Then, the candidate contact material of interest was deposited on the back of each test structure and the cells were finished with evaporated Al. By analysing the current-voltage characteristics of each type of architecture, the carrier selectivity and surface passivation quality of novel contact materials or material stacks can be rapidly screened. To demonstrate the utility of this method, we present a preliminary investigation of nitride compounds as electron-selective contacts in silicon solar cells, in particular zinc tin nitride ($ZnSnN_2$), which is naturally n-type and has favourable band alignments with c-Si. $ZnSnN_2$ was deposited by reactive sputtering as an electron contact on each test structure. No passivation was observed, but decent electron-selectivity was observed when in direct contact with the silicon wafer. When combined with intrinsic amorphous silicon, poor performances were obtained with poor selectivity and the occurrence of an S-shape, likely due to insufficient selectivity of the ZTN. Similar results were obtained for 2 nm and 20 nm thick layers, indicating selectivity did not result from the Al over-layer, but was in fact due to the ZTN itself. Overall, this work shows the three-architecture screening method is a useful tool for assessing novel contact materials for silicon heterojunction solar cells.

INTRODUCTION

Silicon heterojunction (SHJ) solar cells have achieved record high efficiencies by using contact stacks based on thin hydrogenated amorphous silicon (a-Si:H) layers.[1–3] The key to this success lies in combining selective carrier extraction from doped a-Si:H with highly efficient surface passivation from intrinsic a-Si:H. However, the highest efficiencies are obtained for interdigitated back contact (IBC) architectures, which avoid parasitic light absorption in front-side a-Si:H layers. Such parasitic absorption accounts for typically up to 2 mA/cm^2 of current loss in standard SHJ cells.[3,4] Additionally, achieving optimal contact properties in a-Si:H (such as low-recombination together with low-resistance charge extraction) requires finely-tuned processing that is difficult to implement in production. Carrier-selective contact materials with greater transparency and less sensitivity to process variations could help to enable large-scale implementation of SHJ solar cells in industry.

To address the problem of parasitic absorption, researchers have begun exploring transition metal oxide (TMO) materials for use as carrier-selective contacts.[5–10] These materials are wider bandgap than a-Si:H, and when combined with well-known passivation layers, such as intrinsic a-Si:H, can provide reduced parasitic absorption while maintaining selectivity and low contact resistance. One well-known example is molybdenum oxide (MoO_x), which has been successfully applied as a hole-selective contact in SHJ solar cells. However, this material imposes additional limitations on the cell fabrication process, due to its sensitivity to elevated temperature, hydrogen, or plasma exposure.[10,11] As electron-selective contacts, a large variety of materials have been investigated, though their

SiliconPV 2018, The 8th International Conference on Crystalline Silicon Photovoltaics
AIP Conf. Proc. 1999, 040007-1–040007-8; https://doi.org/10.1063/1.5049270
Published by AIP Publishing. 978-0-7354-1715-1/$30.00

successful implementation always relies on the use of finely-tuned thin layers (from below one to a few nanometers) and the presence of a low-work function metal (typically Al but sometimes Mg or Ca) directly on it.[12–17] This approach suggests that the electron selectivity comes, to a great extent, from the metal electrode, and not only from the material itself. Though this has enabled scientifically interesting cell concepts, e.g. with a dopant-free architecture,[18–20] the efficiency of such devices is inherently limited due to the large optical absorption of the Si/Al interface when only a few nanometers of dielectric spacer is used.[21] Also, this precludes the use of such contacts on the light-incident side or for a bifacial cell architecture, which is an appealing feature for large-scale energy production from photovoltaics.[22]

Nitrides are an attractive alternative to oxide materials for carrier selective contacts due to their ability to withstand high temperature processing and plasma exposure.[23,24] Crucially, some nitride materials possess bandgaps wider than 2 eV, making them more transparent than a-Si. Materials such as the III-N family and their alloys, or the more recently developed family of Zn-IV-N_2 materials, are interesting candidates based on advantageous band alignment with crystalline silicon (c-Si) and the possibility for bandgap tuning by alloying.[25–28] Stoichiometric $ZnSnN_2$ exhibits high n-type self-doping (10^{20} cm^{-3}), tunable down to a few 10^{16} cm^{-3}, and an electron affinity near 4.1 eV, which aligns well with the conduction band minimum of c-Si.[25,29] Application of nitride materials as carrier selective contacts in SHJ solar cells remains a largely unexplored topic, with only one other published demonstration,[30] which indicates an opportunity for discovery.

We investigate here as an exemplary material system the implementation of $ZnSnN_2$ as electron-selective contact for c-Si solar cells. Developing new materials for application in a mature technology requires rapid transition between development and application. In this work, we demonstrate a fast and efficient method of screening the carrier selective and passivating potential of any proposed contact material. The method consists of fabricating three architectures, each yielding important information about the test material's contact performance.

METHODS

Thin Film Deposition and Characterization

Four samples of stoichiometric $ZnSnN_2$ were deposited by radio frequency (RF) co-sputtering onto unheated Eagle XG® glass substrates rotating at 90 rpm in a chamber with 10^{-6} Torr residual water base pressure, as confirmed by residual gas analyzer. Deposition times were 5, 10, 20, and 35 minutes, respectively. For all samples, metallic zinc and tin targets inclined at 45° to the substrate normal were used as cation sources, N_2 was used as anion source. A shadow mask consisting of a 4 x 11 grid of rectangular pads was used for each deposition, in order to measure thickness as a function of deposition time by profilometry. Each sample was characterized for cation composition, crystal structure, and transmission and reflection as described in previous work.[31]

Solar Cell Fabrication and Characterization

Solar cells were fabricated on 280-µm-thick, n-type, float-zone wafers textured in a KOH-based solution, cleaned and cleaved into quarters. Directly prior to PECVD of the a-Si:H layers, the native oxide layer was removed from the wafer surface with diluted HF. The front-side of each device was prepared with a p-type a-Si:H contact stack and then finished with ITO sputtering through a shadow mask that defined three 1 cm^2 devices per sample. For the rear side of the samples, two were left bare, two were coated with intrinsic a-Si:H, and two were coated with intrinsic a-Si:H followed by n-type a-Si:H. After finishing the front contact stack, a one-sided HF etch was performed on the rear-side of each sample prior to nitride layer deposition. ZTN layers were then deposited on each set of samples using the deposition parameters described earlier. One set of samples received 2 nm and the other set received 20 nm of ZTN, as determined by deposition time calibrated using profilometry of films grown on glass. Aluminum was then evaporated on the ZTN films, and the samples were annealed at 200 °C for 20 minutes. IV measurements of all cells were performed using a WACOM sun simulator with Keithley sourcemeter and multimeter.

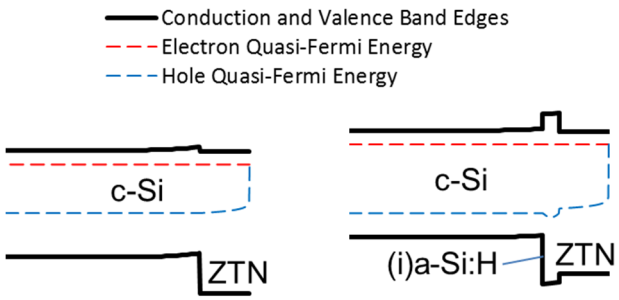

FIGURE 1. Simulated band diagrams for illuminated heterojunction solar cells using a c-Si absorber and a ZTN-based electron-selective contact. Two band diagrams are given, corresponding to a situation with or without a passivating intrinsic a-Si:H layer between the c-Si wafer surface and the nitride electron contact. Band positions for ZTN taken from [25].

RESULTS AND DISCUSSION

Nitride Material Properties

FIGURE 1 shows schematic band alignment of ZTN electron-selective contact both with and without an (i)a-Si:H passivating layer. The band alignment was simulated using PC1D, for which material parameters corresponding to a-Si:H were used for the nitride layer but using bandgap, electron affinity and doping of the actual ZTN material. In view of the assumptions required to construct the simulated diagrams, we emphasize Figure 1 is solely for the purpose of visually comparing band positions. N-type doping was assumed for both cases and a poor carrier lifetime (10^{-4} μs) in the nitride layer. Band positions for ZTN are taken from Ref.[25], in which the ZTN valence band position was determined using X-ray photoelectron spectroscopy. We note that estimating band offsets by comparing the band positions of stand-alone materials (i.e. not in contact in a junction) is prone to error from neglecting the effects of, for example, interface dipoles.[32] For the ZTN films in this work, we are assuming the influence of interface dipole formation is minimized due to the non-oriented, polycrystalline nature of the film microstructure. Based on these band positions, we find that ZTN has an excellent conduction-band alignment with c-Si and an ~0.5 eV valence band offset, which are desirable properties for an electron-selective contact. Introducing an (i)a-Si:H passivating layer introduces a small band offset, though if kept thin enough it could be overcome by thermionic emission, similar to the case of standard silicon heterojunction cells employing an intrinsic/n-type a-Si:H stack. No surface passivation is expected when depositing ZTN directly on the c-Si (a surface recombination velocity (SRV) of 10^5 cm/s was used on the rear side of the c-Si wafer), hence the lower quasi-Fermi-level splitting than for other cases (SRV of 1 cm/s assumed when an (i)a-Si:H layer is introduced).

FIGURE 2 displays an X-ray diffraction (XRD) pattern for 125 nm, stoichiometric ZTN films grown under the same conditions as those used in the test architectures described below. The reference trace (black curve) is an XRD pattern simulated for an orthorhombic ($Pna2_1$) $ZnSnN_2$ structure taken from http://materials.nrel.gov.[33–35] The ZTN films are found to be polycrystalline, with peak positions in excellent agreement with the reference. Orthorhombic supercell peaks ($2\theta = 20°$ and 21°) are not observed, indicating the films in this work exhibit some degree of cation-disorder, which is typical for $ZnSnN_2$.[36]

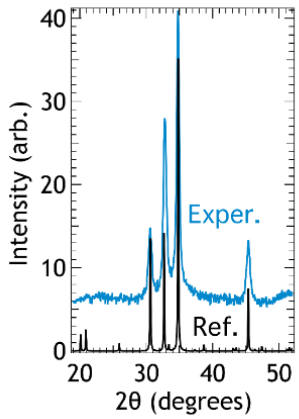

FIGURE 2. XRD of 125 nm thick ZTN grown on glass compared to a reference trace from https://materials.nrel.gov.

FIGURE 3 displays transmission and reflection spectroscopy measurements taken of ZTN at two thicknesses. The ZTN layers were found to be transparent (up to 85% transmission) in the critical 900-1200 nm range, as well as in the blue region of the spectrum if maintained thin enough (less than 50 nm). Stoichiometric ZTN films grown by co-sputtering are known from previous work to be n-type self-doped at a level of 10^{20} cm^{-3},[37] indicating these films are sufficiently conductive for low-resistance charge transport.

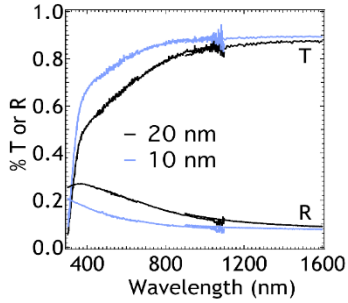

FIGURE 3. Transmission and reflection for two thicknesses of ZTN grown on glass. ZTN is found to be transparent at these thicknesses in the critical 900-1200 nm range.

Passivation and Selectivity Assessment

After initial characterization of the nitride material, a device-oriented rapid and efficient screening approach was followed to investigate its suitability as carrier-selective contacts (CSC). In this approach, three test architectures were used to assess several properties of the material at once. FIGURE 4 shows the three structures and their associated IV curves for the two investigated thicknesses of ZTN. We started from a standard silicon heterojunction architecture and replaced the traditional a-Si:H-based electron-selective contact with a ZTN-based contact. In all three cases, a low work function metal (Al) was used to encourage efficient electron extraction, similar to all non-Si-based electron-selective contact architectures.[12–16] Each configuration allows to probe a specific functionality of the new material: (a) tests the electron selectivity and passivation quality; (b) tests whether the material can impose electron selectivity when combined with a passivating intrinsic a-Si:H layer; and (c) tests whether the contact material forms barriers to electron extraction, either inherently or when in contact with a-Si:H, since passivation and selectivity are provided entirely by the a-Si:H layers. Analysing the current-voltage characteristics of each test structure allows for rapid screening of new contact layers.

In the first test architecture (FIGURE 4a), in which the ZTN layer is in direct contact with the c-Si, V_{oc} up to 560 mV is obtained and fill factor (FF) is ~66%. This V_{oc} value is more than twice the V_{oc} of the c-Si/ITO/Ag reference cell (panel (a), green curve), which has neither passivating nor electron-selective layers in the back contact stack. Thus, the performance of architecture (a) indicates the ZTN layer provides electron selectivity. However, no passivation is observed from the ZTN layers in panel (a), since the V_{oc} is almost 200 mV lower than the all-silicon reference cell shown in panel (c) (green curve). Additionally, little difference in IV characteristic is observed between the two ZTN thicknesses. By choosing two thicknesses for ZTN, the role of the Al capping layer can be decoupled from the effect of the contact layer itself. Either the investigated material functions best as an interface layer, preventing Fermi-level pinning while allowing the Al to impose electron selectivity in the contact stack (then only the thin layer will function), or the layer itself is an efficient electron-selective layer independently of the presence of the Al (in which case the thicker layer will also function). Numerous examples of the former case exist in literature, including LiF, MgF_x, whereas few examples other than n-type silicon are reported for the latter.[12–16] For ZTN, architecture (a) demonstrates the material is inherently electron-selective, and does not rely on the presence of the low work function Al capping layer to impose selectivity.

For the second architecture (FIGURE 4b), the expected voltage increase when inserting the intrinsic a-Si:H passivation layer below the ZTN layer is not observed (V_{oc} is slightly reduced), and a drastic reduction of FF is seen. The drop in FF could have more than one origin, thus it is important to separate any contribution from blocked charge extraction due to detrimental interfacial chemistry between the a-Si:H and the ZTN. To do so, we turn to the third architecture (FIGURE 4c), in which passivation and carrier selectivity are provided by the a-Si:H layers, and ZTN acts only as a spectator. In this configuration, V_{oc} and FF increase compared to architecture (a), meaning that formation of an interface layer or modification of ZTN material properties due to growth on a-Si:H can be ruled out. Returning to analysis of architecture (b), we can conclude that the drop in FF compared to case (a) is due to insufficient selectivity of the ZTN layer. ZTN appears sufficiently selective when used directly on top of the wafer, but not sufficiently to induce selectivity through the intrinsic a-Si:H layer. Such an effect has already been reported for metal-oxide hole-selective contacts.[9,38,39] This suggests that better performance could be obtained by combining the ZTN layer with an alternative passivation layer and highlights the importance of studying various passivating strategies when investigating novel carrier-selective contact layers. FIGURE 5 gives a summary of the V_{oc} and FF values measured for each architecture for ZTN-containing cells. Example analysis that can be drawn from each architecture is given in TABLE 1.

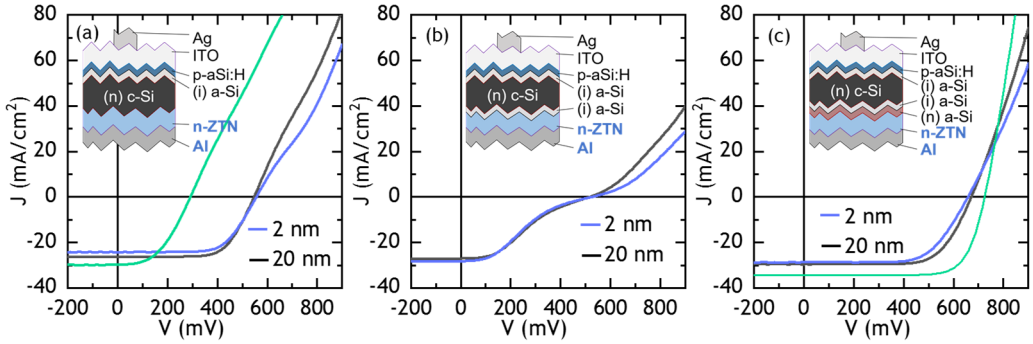

FIGURE 4. Representative IV curves for the three device architectures fabricated with ZTN, each for two thicknesses of the ZTN layer. The green curve in panel (a) corresponds to a reference cell of the same size prepared similarly but with only tin-doped indium oxide (ITO) and Ag as the back contact stack, to demonstrate cell performance without any passivating or electron-selective layers. The green curve in panel (c) is for an all-silicon reference cell (i.e. no ZTN interlayer) with ITO and Ag in place of Al. Insets: schematics showing the three architectures used to screen passivation and carrier selectivity in this work. All references to configurations A, B, or C in the text correspond to the architectures shown in panels (a), (b), and (c) respectively.

TABLE 1. Example interpretation of the possible combinations of results obtained for architectures (a), (b) and (c). The grey box indicates the status of the ZTN layers investigated here.

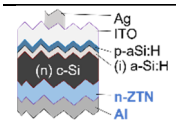	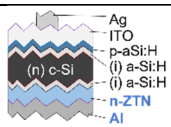	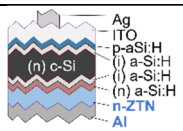	**Interpretation**
Poor performance	Poor performance	Poor performance	Material causes severe limitation to the flow of electrons, should be abandoned (or tried as a hole-selective contact), e.g. (p)a-Si:H.
Poor performance	Poor performance	Good V_{oc}, good FF	Material is not electron-selective, yet does not prevent electron transport. Not promising, e.g. metals and TCOs
V_{oc} > 500 mV	Poor performance	Poor performance	Material is probably electron-selective, yet combination with a-Si:H causes barrier to charge extraction. Could be promising with another passivation layer, e.g. some evaporated MoO_x layers (as hole contact).
V_{oc} >500 mV	Poor performance	Good V_{oc}, good FF	Material is probably electron-selective yet combination with (i)a-Si:H causes loss of selectivity through the (i)a-Si:H layer, indicating the material does not exhibit sufficient degree of carrier selectivity, e.g. ZTN (here).
V_{oc} > 500 mV, good FF	Good V_{oc}, good FF	Good V_{oc}, good FF	Material does not provide passivation, yet is selective and interacts well with a-Si:H. Promising. e.g. some TiO_x layers.
V_{oc} > 600 mV, good FF	Good V_{oc}, good FF	Good V_{oc}, good FF	Material provides some passivation, is selective and can be used with a-Si:H passivation layers. Very promising.

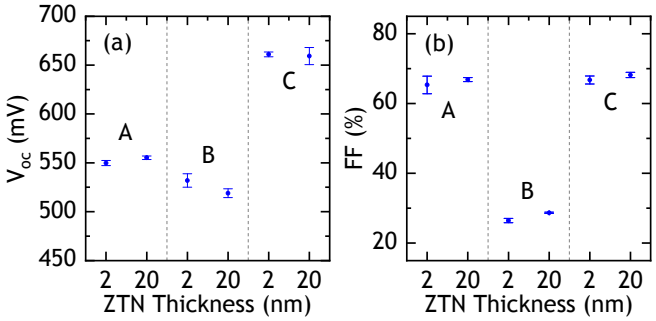

FIGURE 5. Summary of (a) V_{oc} and (b) FF values for the three architectures using ZTN as an electron selective contact. Each pair of values gives the average V_{oc} or FF of three cells of the same architecture with either 2 nm or 20 nm of ZTN. The error bars show the standard deviation among three measurements of nominally identical cells.

CONCLUSION

A three-architecture method for screening new carrier selective contacts (CSCs) for SHJ solar cells was presented. The utility of this method was demonstrated by investigating $ZnSnN_2$-based electron-selective contacts. $ZnSnN_2$ (ZTN) was found to provide electron-selectivity but not passivation. However, the ZTN layer led to an S-shape in the IV curve when tested in combination with an intrinsic a-Si:H passivation layer, suggesting sub-standard electron-selectivity in this configuration. This finding suggests the valence band offset between ZTN and c-Si may not be large enough to impart strong selectivity to a ZTN-based contact. Overall, these results demonstrate a facile method for rapid assessment of new materials' viability as CSCs for SHJ solar cells and point toward avenues for further investigation.

ACKNOWLEDGMENTS

This material is based upon work supported by the U.S. Department of Energy's (DOE) Office of Energy Efficiency and Renewable Energy (EERE) under Solar Energy Technologies Office (SETO) Agreement Number 30302. Additionally, this project has received funding from the European Union's Horizon 2020 research and innovation programme under Grant Agreement No. 727523 (NextBase). Funding from the Swiss national science foundation (SNF) through the Ambizione Energy grant "ICONS" is also acknowledged. We acknowledge Christophe Allebe and Fabien Debrot from CSEM for high quality wet-processing of the silicon wafers.

REFERENCES

1. Masuko, K. *et al.* Achievement of More Than 25% Conversion Efficiency With Crystalline Silicon Heterojunction Solar Cell. *IEEE J. Photovoltaics* **4,** 1433–1435 (2014).
2. Adachi, D., Hernández, J. L. & Yamamoto, K. Impact of carrier recombination on fill factor for large area heterojunction crystalline silicon solar cell with 25.1% efficiency. *Appl. Phys. Lett.* **107,** 233506 (2015).
3. Yoshikawa, K. *et al.* Silicon heterojunction solar cell with interdigitated back contacts for a photoconversion efficiency over 26%. *Nat. Energy* **2,** 17032 (2017).
4. Holman, Z. C. *et al.* Current Losses at the Front of Silicon Heterojunction Solar Cells. *IEEE J. Photovoltaics* **2,** 7–15 (2012).
5. Battaglia, C. *et al.* Silicon heterojunction solar cell with passivated hole selective MoO_x contact. *Appl. Phys. Lett.* **104,** 113902 (2014).
6. Bivour, M., Temmler, J., Steinkemper, H. & Hermle, M. Molybdenum and tungsten oxide: High work function wide band gap contact materials for hole selective contacts of silicon solar cells. *Sol. Energy Mater. Sol. Cells* **142,** 34–41 (2015).
7. Gerling, L. G. *et al.* Transition metal oxides as hole-selective contacts in silicon heterojunctions solar cells. *Sol. Energy Mater. Sol. Cells* **145,** 109–115 (2016).
8. Boccard, M., Ding, L., Koswatta, P., Bertoni, M. & Holman, Z. Evaluation of metal oxides prepared by reactive sputtering as carrier-selective contacts for crystalline silicon solar cells. in *2015 IEEE 42nd Photovoltaic Specialist Conference (PVSC)* 1–3 (IEEE, 2015). doi:10.1109/PVSC.2015.7356167
9. Mews, M., Lemaire, A. & Korte, L. Sputtered Tungsten Oxide as Hole Contact for Silicon Heterojunction Solar Cells. *IEEE J. Photovoltaics* 1–7 (2017). doi:10.1109/JPHOTOV.2017.2714193
10. Geissbühler, J. *et al.* 22.5% Efficient Silicon Heterojunction Solar Cell With Molybdenum Oxide Hole Collector. *Appl. Phys. Lett.* **107,** (2015).
11. Neusel, L., Bivour, M. & Hermle, M. Selectivity issues of MoOx based hole contacts. *Energy Procedia* **124,** 425–434 (2017).
12. Avasthi, S. *et al.* Hole-blocking titanium-oxide/silicon heterojunction and its application to photovoltaics. *Appl. Phys. Lett.* **102,** 203901 (2013).
13. Bullock, J. *et al.* Lithium Fluoride Based Electron Contacts for High Efficiency n-Type Crystalline Silicon Solar Cells. *Adv. Energy Mater.* **6,** 1600241 (2016).
14. Wan, Y. *et al.* Conductive and Stable Magnesium Oxide Electron-Selective Contacts for Efficient Silicon Solar Cells. *Adv. Energy Mater.* (2016). doi:10.1002/aenm.201601863
15. Boccard, M., Yang, X., Weber, K. & Holman, Z. C. Passivation and carrier selectivity of TiO<inf>2</inf> contacts combined with different passivation layers and electrodes for silicon solar cells. in *Conference Record of the IEEE Photovoltaic Specialists Conference*, (2016).
16. Allen, T. G. *et al.* A Low Resistance Calcium/Reduced Titania Passivated Contact for High Efficiency Crystalline Silicon Solar Cells. *Adv. Energy Mater.* **7,** 1602606 (2017).
17. Yang, X., Weber, K., Hameiri, Z. & De Wolf, S. Industrially feasible, dopant-free, carrier-selective contacts for high-efficiency silicon solar cells. *Prog. Photovoltaics Res. Appl.* **25,** 896–904 (2017).
18. Nagamatsu, K. A. *et al.* Titanium dioxide/silicon hole-blocking selective contact to enable double-heterojunction crystalline silicon-based solar cell. *Appl. Phys. Lett.* **106,** 123906 (2015).
19. Wu, W. *et al.* Dopant-free multilayer back contact silicon solar cells employing V_2O_x/metal/V_2O_x as an emitter. *RSC Adv.* **7,** 23851–23858 (2017).
20. Bullock, J. *et al.* Stable Dopant-Free Asymmetric Heterocontact Silicon Solar Cells with Efficiencies above 20%. *ACS Energy Lett.* **3,** 508–513 (2018).

21. Holman, Z. C., De Wolf, S. & Ballif, C. Improving metal reflectors by suppressing surface plasmon polaritons: a priori calculation of the internal reflectance of a solar cell. *Light Sci. Appl.* **2,** (2013).
22. Cuevas, A., Luque, A., Eguren, J. & Alamot, J. Del. 50 per cent more output power from an albedo- collecting flat panel using bifacial solar cells. *Sol. Energy* **29,** (1982).
23. Wang, J., Mulligan, P., Brillson, L. & Cao, L. R. Review of using gallium nitride for ionizing radiation detection. *Appl. Phys. Rev.* **2,** 31102 (2015).
24. Parks, D. A. & Tittmann, B. R. Radiation tolerance of piezoelectric bulk single-crystal aluminum nitride. *IEEE Trans. Ultrason. Ferroelectr. Freq. Control* **61,** 1216–1222 (2014).
25. Arca, E. *et al.* Band Edge Positions and Their Impact on the Simulated Device Performance of ZnSnN2-Based Solar Cells. *IEEE J. Photovoltaics* **8,** 110–117 (2018).
26. Punya, A. & Lambrecht, W. R. L. Band offsets between $ZnGeN_2$, GaN, ZnO, and $ZnSnN_2$ and their potential impact for solar cells. *Phys. Rev. B* **88,** 75302 (2013).
27. Wang, T., Ni, C. & Janotti, A. Band alignment and p-type doping of $ZnSnN_2$. *Phys. Rev. B* **95,** 205205 (2017).
28. Fioretti, A. N. "Development of Zinc Tin Nitride for Application as an Earth-Abundant Photovoltaic Absorber," Ph.D. Thesis, Colorado School of Mines, 2017.
29. Fioretti, A. N. *et al.* Effects of Hydrogen on Acceptor Activation in Ternary Nitride Semiconductors. *Adv. Electron. Mater.* **3,** 1600544 (2017).
30. Yang, X. *et al.* Tantalum Nitride Electron-Selective Contact for Crystalline Silicon Solar Cells. *Adv. Energy Mater.* 1800608 (2018). doi:10.1002/aenm.201800608
31. Fioretti, A. N., Toberer, E. S., Zakutayev, A. & Tamboli, A. C. Effects of low temperature annealing on the transport properties of zinc tin nitride. in *2015 IEEE 42nd Photovoltaic Specialist Conference (PVSC)* 1–5 (IEEE, 2015). doi:10.1109/PVSC.2015.7355694
32. Korte, L., Rößler, R. & Pettenkofer, C. Direct determination of the band offset in atomic layer deposited ZnO/hydrogenated amorphous silicon heterojunctions from X-ray photoelectron spectroscopy valence band spectra. *J. Appl. Phys.* **115,** 203715 (2014).
33. Lany, S. Semiconducting transition metal oxides. *J. Phys. Condens. Matter* **27,** 283203 (2015).
34. Lany, S. Band-structure calculations for the 3d transition metal oxides in GW. *Phys. Rev. B* **87,** 85112 (2013).
35. Stevanović, V., Lany, S., Zhang, X. & Zunger, A. Correcting density functional theory for accurate predictions of compound enthalpies of formation: Fitted elemental-phase reference energies. *Phys. Rev. B* **85,** 115104 (2012).
36. Martinez, A. D., Fioretti, A. N., Toberer, E. S. & Tamboli, A. C. Synthesis, structure, and optoelectronic properties of II–IV–V_2 materials. *J. Mater. Chem. A* **5,** 11418–11435 (2017).
37. Fioretti, A. N. *et al.* Combinatorial insights into doping control and transport properties of zinc tin nitride. *J. Mater. Chem. C* **3,** (2015).
38. Boccard, M., Ding, L., Koswatta, P., Bertoni, M. & Holman, Z. Evaluation of metal oxides prepared by reactive sputtering as carrier-selective contacts for crystalline silicon solar cells. in *2015 IEEE 42nd Photovoltaic Specialist Conference, PVSC 2015* (2015). doi:10.1109/PVSC.2015.7356167
39. Messmer, C., Bivour, M., Schon, J., Glunz, S. W. & Hermle, M. Numerical simulation of silicon heterojunction solar cells featuring metal oxides as carrier-selective contacts. *IEEE J. Photovoltaics* **8,** 456–464 (2018).
40. Stevanović, V., Lany, S., Ginley, D. S., Tumas, W. & Zunger, A. Assessing capability of semiconductors to split water using ionization potentials and electron affinities only. *Phys. Chem. Chem. Phys* **3706,** 3706–3714 (2014).